NIH Public Access
Author Manuscript
Light Sci Appl. Author manuscript; available in PMC 2014 February 11.

Published in final edited form as:
Light Sci Appl. 2013 ; 2: . doi:10.1038/lsa.2013.24.

Laser patterning for the study of MSC cardiogenic differentiation at the single-cell level

Zhen Ma[*,1,2], **Qiuying Liu**[*,3], **Huaxiao Yang**[1], **Raymond B Runyan**[4], **Carol A Eisenberg**[5], **Meifeng Xu**[6], **Thomas K Borg**[7], **Roger Markwald**[7], **Yifei Wang**[3], and **Bruce Z Gao**[*,1]

[1]Department of Bioengineering and COMSET, Clemson University, Clemson, SC 29634, USA

[2]Department of Bioengineering, University of California, Berkeley, Berkeley, CA, USA

[3]Biomedical R&D Center, Jinan University, Guangzhou, China

[4]Department of Cellular and Molecular Medicine, University of Arizona, Tucson, AZ 85724, USA

[5]New York Medical College/Westchester Medical Center Stem Cell Laboratory, New York Medical College, Valhalla, New York, USA

[6]Department of Pathology and Laboratory Medicine, University of Cincinnati Medical Center, Cincinnati, OH, USA

[7]Department of Regenerative Medicine and Cell Biology, Medical University of South Carolina, Charleston, SC, USA

Abstract

Mesenchymal stem cells (MSCs) have been cited as contributors to heart repair through cardiogenic differentiation and multiple cellular interactions, including the paracrine effect, cell fusion, and mechanical and electrical couplings. Due to heart–muscle complexity, progress in the development of knowledge concerning the role of MSCs in cardiac repair is heavily based on MSC–cardiomyocyte coculture. In conventional coculture systems, however, the *in vivo* cardiac muscle structure, in which rod-shaped cells are connected end-to-end, is not sustained; instead, irregularly shaped cells spread randomly, resulting in randomly distributed cell junctions. Consequently, contact-mediated cell–cell interactions (e.g., the electrical triggering signal and the mechanical contraction wave that propagate through MSC–cardiomyocyte junctions) occur randomly. Thus, the data generated on the beneficial effects of MSCs may be irrelevant to *in vivo* biological processes. In this study, we explored whether cardiomyocyte alignment, the most important phenotype, is relevant to stem cell cardiogenic differentiation. Here, we report (i) the construction of a laser-patterned, biochip-based, stem cell–cardiomyocyte coculture model with controlled cell alignment; and (ii) single-cell-level data on stem cell cardiogenic differentiation under *in vivo*-like cardiomyocyte alignment conditions.

Keywords

cardiogenic differentiation; mesenchymal stem cells; microenvironment; optical force; single-cell analysis

© 2013 CIOMP. All rights reserved

This work is licensed under a Creative Commons Attribution-NonCommercial-Share Alike 3.0 Unported License. To view a copy of this license, visit http://creativecommons.org/licenses/by-nc-sa/3.0

Correspondence: Professor BZ Gao, Department of Bioengineering and COMSET, Clemson University, 201-3 Rhodes Hall, Clemson, SC 29634, USA. zgao@clemson.edu.
*These authors contributed equally to this manuscript.

NIH-PA Author Manuscript
NIH-PA Author Manuscript
NIH-PA Author Manuscript

NIH-PA Author Manuscript

NIH-PA Author Manuscript

NIH-PA Author Manuscript

INTRODUCTION

The genes and surrounding environment of a cell regulate its function. The interplay between the complex process of gene expression and microenvironmental intricacies causes large functional variation, even among cells within a small region of tissue. For example, by patterning human mesenchymal stem cells (MSCs), it was found that their differentiation was related to both geometries[1] and surface stiffness.[2] Even within one patterned colony, MSCs underwent a higher percentage of osteogenesis on the edge of the pattern than in the center, which indicating that MSC differentiation was directed by microenvironmental cues.[3] Recent studies have revealed that cell culture models that provide a microenvironment significantly different from that observed in *in vivo* tissue cause deviations in cell response and behavior.[4] Therefore, researchers have made efforts to understand the intercellular variability of gene expression and cellular behavior in response to surrounding stimuli, especially the tissue-specific, *in vivo*-mimicking microenvironment. For example, bio-MEMS techniques have been developed to create an engineered cell culture for systematic observation of the interactions of cells with their surroundings, including interactions with the adjacent extracellular matrix.[5] Additionally, laser single-cell microdissection techniques have been developed for harvesting single cells from the culturing environment for various biological assays.[6] Further, various single-cell polymerase chain reaction (PCR) techniques[7] are capable of assessing gene expression intercellular variability and correlating the result to the specific microenvironments.[8]

In several clinical trials, MSCs have been used as a stem cell therapy for myocardial infarction by generating functional cardiac tissue, enhancing cardiac function and relieving heart failure symptoms.[9–11] Due to heart muscle complexity, progress in the development of knowledge concerning the role of MSCs in cardiac repair is heavily based on MSC–cardiomyocyte coculture. In conventional coculture systems, however, the *in vivo* cardiac muscle structure, in which rod-shaped cells are connected end-to-end, is not sustained; instead, irregularly shaped cells spread randomly, causing randomly distributed cell junctions. Consequently, contact-mediated cell–cell interactions (e.g., the electrical triggering signal and the mechanical contraction wave that propagate through MSC–cardiomyocyte junctions) occur randomly. Thus, data generated regarding the beneficial effect of MSCs may be irrelevant to *in vivo* biological processes. In this study, we applied a novel laser cell patterning technique to explore whether the alignment of cardiomyocytes, which are the most important feature of cardiac tissue, is relevant to stem cell cardiogenic differentiation.

Although methods to align cardiomyocytes on different substrates have been discussed in a variety of publications, the effects of cardiomyocyte alignment on stem cell cardiogenic differentiation have not been reported. A microabrasion technique was used to align MSCs relative to a randomly cultured cardiomyocyte construct.[12] It was found that the electrical signal propagated faster along the MSCs that were aligned parallel to the boundary of the cardiomyocyte construct than along those that were perpendicular to the boundary. In addition to the suggestion regarding the role of alignment in the formation of more *in vivo*-like cell junctions, these data mainly demonstrate the influence of cell orientation on MSC electrophysiological modulation. In another study, the creation of cellular bridges between cardiac muscle fibers allowed for a comparison of different cell types, including MSCs, to determine the best electrical compatibility with aligned cardiomyocytes.[13]

These reported cell alignment techniques were able to create cell structures using a large number of cells to mimic the native cardiac tissue; thus, they could not be used to explore the importance of alignment on MSC cardiogenic differentiation at the single-cell level.

NIH-PA Author Manuscript

NIH-PA Author Manuscript

NIH-PA Author Manuscript

From a biological point of view, single-cell analyse are important because they include the plasticity and diversity features of stem cells. From a clinical point of view, the importance is that stem cell transplantation experimentation always results in the observation of a single stem cell; thus, only *in vitro* data at the single-cell level are compatible. In one study, which was conducted to achieve a single-cell analysis on MSC–cardiomyocyte interactions, a microcontact-printing method was used to create single-cell islands upon which only one MSC and one cardiomyocyte could attach.[14] However, in such a single-cell assay, cardiomyocyte alignment could not be achieved because the current techniques for surface patterning cannot simultaneously realize single-cell analysis and alignment of a large amount of cardiomyocytes.

There is no technology readily available to researchers that can be used to place a particular cell into a microculturing environment with accurate time and site controls for systematic and repeatable single-cell studies. Hence, it is vital to develop a single-cell manipulation technique that can place single cells into a specific microenvironment with high temporal and spatial resolution. Such a technique, in combination with the established techniques described above, would be invaluable to understanding the single-cell origins of disease states and the cell biology necessary for normal physiology.

In this study, we explore the application of our laser-guided cell micropatterning (LGCM) system[15] in combination with surface patterning methods[16] to investigate stem cell differentiation at the single-cell level in a cardiomyocyte microculturing environment. In previous studies, we determined the effect of cell–cell contact on MSC cardiogenic differentiation by creating a microenvironment with only one MSC and one cardiomyocyte using the LGCM system.[17] In the study reported here, we first constructed a cardiomyocyte culture model with the controlled alignment of cardiomyocyte constructs, and then utilized LGCM to trap and deposit individual MSCs into the constructed model. Next, we evaluated cell differentiation at the single-cell level through single-cell RT-qPCR and patch-clamp assays. Consequently, we report (i) the construction of a laser-patterned, biochip-based, stem cell–cardiomyocyte coculture model with controlled cell alignment; and (ii) single-cell-level data on stem cell cardiogenic differentiation under an *in vivo*-like cardiomyocyte alignment conditions.

A great deal of attention is currently directed at single-cell analysis in current biomedical research because many cell (e.g., cancer and stem cell)-based biological systems that have been recently recognized as critical to human health are dependent on single-cell behaviors. Scientists have long sought a single-cell analytical tool that can be used to place an individual cell into an existing cell culture and then remove the cell to achieve single-cell analysis (e.g., to study the soil and seed model). The contribution of this study is the achievement, for the first time, of accurately placing a single cell into a cell culture niche and then realizing single-cell PCR analysis of the cell through a laser micropatterning technique.

MATERIALS AND METHODS

Optical force simulation

Light has momentum in the direction of its propagation. As light acts against a biological cell, the light's momentum changes due to scattering. According to momentum conservation, the cell must undergo an equal and opposite momentum change, which creates an optical force that acts on the cell. The LGCM technique takes advantage of the optical force to confine a cell in the axis of a laser beam and to propel it along the axis of the beam to the substrate. This process allows for the precise placement of individual cells.

NIH-PA Author Manuscript

NIH-PA Author Manuscript

NIH-PA Author Manuscript

Theoretical simulation of the optical forces is critical for understanding the principle of LGCM and designing an effective LGCM system. The geometric optics simulation introduced by Ashkin[18] provided a visualization of the optical force distribution in a single-beam optical trap for a sphere of significantly greater diameter in comparison to the wavelength. A typical biological cell in suspension has a diameter in the range of 5–20 μm. For spheres with a diameter in this range, wave effects become influential during their interactions with light. Without accounting for wave effects, a geometric optics-based method is unable to give an accurate description of laser guidance; thus, wave optics-based methods must be developed.

The optical forces can be determined based on the wave optics for a typical laser beam with a Gaussian profile; accordingly, the generalized Lorenz–Mie theory (GLMT) incorporates all of the effects of light–particle interactions.[19] Based on Ricatti–Bessel and the spherical harmonic functions, GLMT first derives the infinite series representation of the incident and scattered fields. Second, GLMT solves the scattering coefficients (a_n, b_n) by evaluating the boundary conditions at the particle surface. Third, GLMT derives the exact expression of the radial component of the incident Gaussian beam, and finally, it calculates the Gaussian beam expansion coefficients ($g_{n,\mathrm{TE}}$, $g_{n,\mathrm{TM}}$). Given the expansion coefficients for a particular Gaussian beam, the optical forces can be calculated:

$$F_i = C_i \frac{2n_{\mathrm{medium}} P}{\pi \omega_0^2 c}$$

where i=x, y or z, which indicates the radial optical force ($F_{x\mathrm{ory}}$) or axial optical force (F_z); ω_0 is the waist of the laser beam; P is the laser power; c is the speed of light; n_{medium} is the refractive index of the medium; and C_i is the cross-section of the radiation pressure, normalized to the unit of irradiance (i.e., the beam intensity), which represents the amount of energy removed from a unit of irradiance for each unit of time because of scattering in either the radial direction ($C_{x\mathrm{ory}}$) or in the axial direction (C_z).

According to GLMT theory, the beam waist (ω_0) is one of the important parameters in determining the strength and distribution of the optical force. Thus, the optical force distributions along the axial (−200–200 μm) and the radial (−10–10 μm) directions were calculated against different beam waists based on GLMT[20] to estimate a proper beam waist range. The calculations used the parameters of λ=800 nm, P=200 mW, the average cell size=15 μm, the refractive index of the media=1.33 and the average refractive index of the cell=1.36.

The laser-guided cell micropatterning system

We built our LGCM system (Figure 1) based on a stationary laser beam that was vertically focused into the cell deposition chamber to produce a guidance region in which a cell was confined radially and then pushed axially to the substrate along the direction of light propagation. The guidance laser was a Ti-sapphire laser (Spectra-Physics 3900S CW) tuned to a wavelength of 800 nm. The laser beam was expanded and collimated using an NIR achromatic lens pair (f=30 and 150 mm) before passing a dichroic beam splitter. The beam was then focused by a long-working-distance objective (20×, Mitutoyo Plan Apo Infinity-corrected) to generate the guidance region; the objective served as both the guidance lens and the imaging objective. The illumination required for imaging was achieved using a collimated green LED (530 nm, 200 mW) focused onto the substrate inside the chamber by achromatic doublets (f=100 mm). A CCD camera was used to capture the image, which was formed by the Mitutoyo objective after passing the dichroic beamsplitter, a number of infrared filters and a tube lens to eliminate the guidance beam. To align the image's center to

NIH-PA Author Manuscript

NIH-PA Author Manuscript

NIH-PA Author Manuscript

the focal point of the laser beam, the CCD camera was fixed onto a three-dimensional (3D) translational stage; therefore, the beam's guidance region coincided with the imaging system's object plane.

To control the temperature, CO_2 and humidity for long-term cell culturing, both during and after the cell deposition process, a microscope stage incubator (Okolab Electric Warner Instruments, Hamden, CT, USA) was modified to be part of the cell-deposition chamber, which was fitted for a 35-mm Petri dish or a standard multielectrode array with a ring. A #1 coverslip served as the optical window to seal the cell-deposition compartment and to reduce the convection force. The patterning substrate (e.g., a biochip) was placed into the cell deposition chamber, which was controlled by a three-axis motorized translational stage with the maximum horizontal (150 $\mu m\ s^{-1}$) and vertical (50 $\mu m\ s^{-1}$) guidance speeds to maintain the cell within the guidance region.

The cell suspension was pumped into the cell-deposition chamber through a hollow fiber, coupled with a 50 μl microsyringe. The microinjection process was optimized based on the volume (~50 nl) and speed (~25 nl s^{-1}) for injecting the smallest cell number. The cell injection site (i.e., the exit point of the hollow fiber) was not placed directly above the patterning region, which ensured that the injected cells that were not captured by the laser beam would not fall onto the patterning region. Therefore, the guidance region (also the imaging region of the objective) was initially focused onto the injection region by controlling the movement of the cell deposition chamber. Once a cell was trapped at the guidance region of the laser beam, it was instantly pushed downward along the beam axis and thus gradually fell out of focus. The cell was then moved towards the imaging region of the objective by lifting the chamber during guidance for continuous image tracking, which created a relative motion of the cell towards the bottom. Simultaneously, the cell was moved horizontally to the deposition site on the substrate by translating the motorized stage. The chamber navigation was manually controlled through an XBox360 controller with custom-designed LabView software.

Cell culture preparation

Cardiomyocytes were isolated and gathered from 3-day-old neonatal rats using a 2-day protocol. After dissection, the left ventricles were collected and minced in Moscona's saline. Then, the minced ventricles were transferred into 50 ml Dulbecco's phosphate-buffered saline medium with 4 mg trypsin and 50 mg neutral protease, followed by refrigeration overnight at 4 ºC. The next day, the heart tissue was placed in 50 ml Kreb's Ringers bicarbonate buffer medium with 10 mg collagenase type I and 30 mg collagenase type II, followed by agitation in a water bath for 1 h at 50 r min^{-1}. The cell suspension was washed twice using a cardiomyocyte culture medium (Dulbecco's modified Eagle's medium (DMEM high glucose) with 20% fetal bovine serum and 1% penicillin streptomycin) to remove the enzyme residue. The isolated cells were transferred into a 150 cm^2 flask for pre-attachment to remove the cardiac fibroblasts. After 2 h, the unattached cardiomyocytes were collected for subsequent use. Because of the difference in size between cardiomyocytes and non-myocyte cells, we were able to select and deposit only cardiomyocytes into the microwells during the laser-patterning procedure.

Commercial rat bone marrow mesenchymal stem cells (rMSCs; ScienCell™ Research Laboratories, Carlsbad, CA, USA) were characterized with antibodies to CD73, CD90, CD105 and oil red staining after adipocyte differentiation. We maintained the rMSCs using ScienCell's mesenchymal stem cell medium and laser patterned them before Passage V. During and after the laser patterning procedure, the cardiomyocyte culture medium was used as the biochip coculture medium. All procedures using animals complied with pertinent laws

NIH-PA Author Manuscript

NIH-PA Author Manuscript

NIH-PA Author Manuscript

and institutional guidelines. These experiments were approved by Clemson University's Institutional Animal Care and Use Committee through protocol AUP2010-032.

Building biochips

The biochip-based coculture models were constructed by fabricating microwells on biochips, seeding the microwells with cardiomyocytes, and laser-patterning single MSCs into each microwell (Figure 2). For each biochip, identical 4×8 microwells were created by attaching a microfabricated polydimethylsiloxane elastomeric membrane with clear holes onto a glass coverslip.[21] The microwell that promoted cellular alignment was rectangular (measuring 200 μm long and 25 μm wide) so that the geometrical restriction would produce cardiomyocyte alignment. The microwell used to prevent alignment was circular with a diameter of 80 μm. The area of the circular microwell was the same as that of the rectangular microwell (approximately 5000 μm^2). The depth of each microwell was 40 μm to restrict the cell bodies. The cardiomyocytes were seeded into the biochips immediately after cell harvesting (day 1). The dead cells and cell debris were gently washed away after 12 h of incubation. After 3-day culturing (day 4), the cardiomyocytes had fully spread inside the microwells. To achieve single-cell analysis of the stem cell cardiogenic differentiation process, LGCM was used to deposit one rMSC per microwell on the biochip (day 4). To distinguish rMSCs from cardiomyocytes in the biochips, the rMSCs were labeled with membrane-tracking dye, DiI (Vybrant Multicolor Cell-Labeling Kit; Invitrogen, Grand Island, NY, USA), before the laser-patterning procedure. On day 10, all biochips with the same cell-alignment condition were arbitrarily divided into three groups for three types of tests: immunostaining, single-cell PCR or patch clamp.

Immunocytochemistry

Immunostaining was performed on the first group to visualize cell alignment (through sarcomeric α-actinin staining) and to evaluate electrical coupling between rMSCs and cardiomyocytes (through Cx 43 staining). The cells were fixed in 4% paraformaldehyde (15 min), permeabilized in 0.1% Triton X-100 (10 min) and blocked in 2% bovine serum albumin with 4% goat serum (30 min). Next, the cells were incubated with a primary antibody diluted in phosphate-buffered saline (PBS; mouse anti-sarcomeric α-actinin (1 : 400) and rabbit anti-connexin 43 (1 : 200)) at 4 ºC overnight. A triple wash in PBS removed excess primary antibody, and the cells were stained with Cy3-conjugated anti-rabbit IgG at a dilution of 1 : 100 in PBS at room temperature for 2 h. Following removal of the secondary antibody by three washes with PBS, the slides were prepared with the ProLong antifade kit mounting medium and DAPI staining (Invitrogen Inc., New York, USA).

We imaged immunostained cells using a confocal microscope (Eclipse Ti; Nikon, Tokyo, Japan) with a 40× oil-immersed objective, a high sensitivity quantitative monochrome camera (Cool-Snap HQ2; Photometrics, Tucson, AZ, USA), and Nikon imaging software (for image acquisition only). The statistical data were represented as '(the mean±s.d.)%, *n*'. The percentage was determined for each biochip by dividing the number of microwells with the rMSCs that had the characteristic of interest (e.g., Cx 43 expression, inward current formation, *etc*.) by the number of microwells with viable coculture. The total number of biochips was *n*, and the mean and standard deviation were calculated based on all biochips with the same cell-alignment condition.

Single-cell RT-qPCR

Single-cell RT-qPCR was conducted on the second group of biochips. This process was accomplished with a single-cell collection system and a conventional RT-qPCR system. The single-cell collection system was built on a fluorescence microscope with a 10× objective and a long working distance 40× objective, a micropipette holder controlled by a motorized

NIH-PA Author Manuscript

NIH-PA Author Manuscript

NIH-PA Author Manuscript

3D micromanipulator and a custom-fabricated micropipette connected with a 10-ml syringe, as shown in Figure 5a. Borosilicate glass micropipettes were manipulated with a Brown-Flaming puller (P-97; Sutter Instrument Co., Novato, CA, USA) to achieve a tip measuring 15–20 μm in diameter. The micropipette was bent to 30–40º using tweezers under heating with a Bunsen burner flame, so that the edge of the micropipette's opening could be visualized above the target cell under the microscope.

Before cell collection, the micropipette was immersed in PBS solution to allow a small amount of PBS to be sucked into the micropipette by surface tension. The protrusion of the micropipette into the cell-culture dish was initially monitored with a 10× objective and then with a 40× objective to ensure accurate target-cell searching. After the target cell was approached, 10 μl 0.25% trypsin was added to its surroundings, and then the target cell was collected with strong suction. The collected cells were transferred into the lid of a PCR tube with 2 μl RNaST lysis buffer (RNase inhibitor: 2 μg μl^{-1} (Ambion, Austin, TX, USA); NaCl: 0.135 M; Tris-HCl (pH=8.0): 9 mM; dithiothreitol: 4.5 mM).

The One-step RT-qPCR Kit (SuperScript III Platinum SYBR Green; Invitrogen) was used to analyze the individually collected cell. The target gene, GATA4 (F 5′-GCA GCA GCA GCA GTG AAG AG-3′; R 5′-GCA CTG GAT GGA TGG AGG AC-3′), is a transcriptional factor that is expressed in cardiomyocytes during early development. The relative real-time RT-qPCR quantification of gene expression for each sample was achieved by comparing the target-amplified product with GAPDH (F5′-GAG ACA GCC GCA TCT TCT TG-3′; R 5′-GGT AAC CAG GCG TCC GAT AC-3′) within the same sample. The cycle threshold (*C*t) was determined, and the relative expression of GATA4 in rMSCs was analyzed using the $2^{-\Delta\Delta Ct}$ method.

Patch clamp

We evaluated the outcome of cell alignment on the cardiogenic regulation of rMSC electrical properties in the biochip-based assay by performing patch-clamp experiments on the third group of biochips at day 10. Borosilicate glass electrodes were manipulated with a Brown-Flaming puller (P-97; Sutter Instrument Co.) to achieve a tip resistance of 3–4 MΩ when the tip was filled with the pipette solution. We performed the patch-clamp experiments with a computer-controlled current/voltage clamp (Multichannel 700A; Axon Instruments Co., Union City, CA, USA) and a 16-bit data acquisition system (Digidata 1322A; Axon Instruments Co.) with slowly circulating medium held at 37 ºC. The pipette solution contained 140 mM K-gluconate, 1 mM EGTA, 2 mM $MgCl_2$, 2 mM Na_2ATP, and 10 mM HEPES (pH=7.2, 330 mOsm). The bath solution contained 139 mM NaCl, 3 mM KCl, 17 mM $NaHCO_3$, 12 mM glucose, 3 mM $CaCl_2$, 1 mM $MgCl_2$ and 10mM HEPES (pH=7.2, 330 mOsm). After the whole-cell patch was established, the membrane potential was kept at −70 mV with a voltage-step protocol from −70 mV to 20 mV (10 mV increment), and the current signals were acquired.

RESULTS AND DISCUSSIONS

Our optical force simulation data (Figure 3) based on the GLMT displays the axial and radial force distributions along the axial and radial directions with beam waists of 2 and 4 μm. When the beam waist is smaller than 2 μm (not shown in the figure), the axial force changes along the axial direction from negative to positive at all longitudinal sections (planes parallel to the beam axis), which forms the laser tweezers mode.[22] Working in this mode, the laser beam traps the cells around its focal point rather than guiding the cells to move along the beam axis. Because rapid relative motion between the trapped particle and the laser beam is always actively created in the laser patterning procedure, a large radial trapping range is required to provide sufficient trapping force even when the trapped particle

NIH-PA Author Manuscript

NIH-PA Author Manuscript

NIH-PA Author Manuscript

is away from the optimal trapping region during laser beam navigation. Our laser cell micropatterning experiment, in which a cell in cell suspension was trapped and guided by the focused laser beam in the cell deposition chamber, was consistent with the simulated results. The experiment showed that the limited trapping range in the laser tweezers mode did not allow the trapped cell to follow the rapid 3D movement of the laser beam during high-speed patterning navigation in a large volume of cell culture medium with strong convectional flow. When the beam waist was as large as 4 μm, the axial optical force remains positive along the axial direction in all longitudinal sections (Figure 3c), forming the pure-guidance mode. In this particular mode, the radial force was too small (Figure 3d) to confine the cell within the beam axis during the patterning navigation process.

Notably, when the beam waist was 2 μm, the axial force was in the laser tweezer mode only in the longitudinal sections in proximity to the beam axis; elsewhere, the force switches to guidance mode in which the values in the outside longitudinal sections are all positive. We named this working mode the ‘transitional mode’. This transitional mode provides not only a sufficient radial trapping force for cell capture but also the necessary force range for laser navigation with the trapped cell. The transitional mode predicted by our simulation was achieved by our optical system design. In practice, as described in the section on ‘Laser-guided cell micropatterning’, by controlling the speed of the 3D chamber navigation in real time, the cell is maintained in an optimized location where both the radial trapping and the axial guidance forces remain near their maximum values.

Our imaging data showed that the cardiomyocytes inside the rectangular microwells exhibited elongated morphology and that their myofibrils (visualized by α-actinin staining) were aligned in parallel with the microwell’s longitudinal axis (Figure 4a). The cardiomyocytes inside the circular microwells spread along the circle’s radius, with randomly aligned myofibrils. One day after the laser patterning procedure, the rMSCs inside both types of microwells had spread so that their morphologies resembled the surrounding cardiomyocytes within the same microwell, i.e., they were aligned in parallel inside the rectangular microwells (Figure 4b) and oriented randomly inside the circular microwells (Figure 4c).

Cx 43 staining was used to demonstrate the potential electrical coupling between the rMSCs and cardiomyocytes within the same microwells. Cx 43 was expressed as a line shape at the contact area between an rMSC and its adjacent cardiomyocyte inside a rectangular microwell (Figure 4d), in contrast, it was expressed in a distributed fashion inside the circular microwells (Figure 4e). No significant difference was observed in Cx 43 expression (the percentage expressed among the total number of samples) between the aligned (36% ±5.9%, n=20) and non-aligned (34%±7.7%, n=20) models. However, the distribution of Cx 43 in the rectangular microwells resembled the native structure: line-shape along the end-to-end and side-to-side interfaces (Figure 4d). The line-shaped Cx 43 expression suggests that gap junctions have formed between the rMSCs and the surrounding cardiomyocytes. This effect may establish electrical communication between the cells, which may facilitate the electrical property regulation of the stem cell, as shown by the patch clamp and the single-cell PCR data described below. In the circular microwells, Cx 43 was expressed in a distributed pattern, which suggests a reduced likelihood of electrical coupling. This result may partially explain the weaker regulation of the rMSC electrical properties in the circular microwells than in the rectangular microwells.

In some rectangular microwells (∼4%), the rMSCs were fused with their adjacent cardiomyocytes, forming a hybrid cell with a double nucleus, a DiI-labeled cell membrane and a sarcomeric structure, as shown in Figure 4f and 4g. This cell fusion phenomenon was

NIH-PA Author Manuscript

NIH-PA Author Manuscript

NIH-PA Author Manuscript

not found in the circular microwells, which suggests that the *in vivo*-like cell alignment facilitated the rMSC process of acquiring a cardiac structure through cell fusion.

The laser-deposited stem cell in each microwell was collected using a glass micropipette (Figure 5a). To visualize the gene expression profile in a population of cells, the distributions of GATA4 expression (in logarithmic scale) among 30 single-cell samples were plotted as histograms (Figure 5b–5d) for rMSCs in the aligned and non-aligned groups and for cardiomyocytes (control). The variation of gene expression shown in the histograms indicates that single-cell RT-qPCR provided a tool for investigating the biological variation among the rMSCs under the same microenvironment. When the distribution in the aligned coculture is compared with that in the random coculture model, even when accounting for the variations among single cells, the aligned coculture model shifts towards that of the cardiomyocytes, suggesting that the *in vivo*-like cell alignment promoted the car-diogenic regulation of rMSC differentiation.

The inward currents associated with an action potential are essential for the excitation and contraction of cardiomyocytes. Therefore, the appearance of inward currents is considered a specific indication of the cardiogenic regulation of rMSC electrical properties.[23] In the rectangular microwells, 34%±5.3% (n=20) of rMSCs exhibited inward currents, whereas 24%±4.9% (n=20) of rMSCs in the circular microwells exhibited inward currents. In patch-clamp experiments, we detected large inward currents of the cocultured cardiomyocytes, starting at −60 mV and reaching a peak value (−56±12.2 pA pF^{-1}) at −40 mV. The inward currents of rMSCs in the rectangular and circular microwells started at −40 mV and reached a peak value at −10 mV, as shown in Figure 6. In our previous findings, among the various ion channels that are related to inward currents, only the calcium channel gene was extensively expressed in the rMSCs cocultured with cardiomyocytes. This may explain the shift toward zero for the current that corresponds to the peak value of the *I–V* curve obtained from the rMSCs in comparison with that obtained from the cardiomyocytes. Additionally, the peak value of the inward current density of the rMSCs in the rectangular microwells (−29±6.8 pA pF^{-1}, n=20) was significantly higher (P<0.05) than that of the rMSCs in the circular microwells (−22.3±4.9 pA pF^{-1}, n=20). These findings indicate that parallel-cell alignment, an *in vivo*-like phenotype, facilitated the cardiogenic modulation of the rMSC electrical properties.

CONCLUSIONS

For the first time, we collected and analyzed a single cell that had been placed into a microfabricated cell culture environment using a laser beam. We determined the optimal configuration for laser patterning; that is, the beam should be configured in a focus mode that is transitional, from a laser trap mode to a laser guidance mode. Our data demonstrate that this laser-patterned, biochip-based stem cell–cardiomyocyte coculture model can be used to study the cell–cell interaction that causes the cardiogenic differentiation of rMSCs. The cells inside the rectangular microwells exhibited a parallel-aligned morphology, whereas the cells inside the circular microwells exhibited a random morphology. This system provides a variety of analytical tools that are essential to defining the morphological and physiological properties of rMSCs during differentiation. These tools, including single-cell RT-qPCR and patch clamp, profile the individual variations inside the heterogeneous rMSC population in response to the microenvironmental and cell–cell interactions. The data show that the *in vivo*-like, aligned morphology facilitated the rMSC acquisition of a cardiac-specific contractile cytoskeleton, transcription factors, a connexin 43 distribution and electrophysiological properties.

NIH-PA Author Manuscript

NIH-PA Author Manuscript

NIH-PA Author Manuscript

Acknowledgments

This work was partially supported by NIH (SC COBRE P20RR021949, Career Award 5k25hl088262-04 and 5R01 HL085847); NSF (MRI, CBET-0923311 and SC EPSCoR RII EPS-0903795 through SC GEAR program); and Guangdong Provincial Department of Science and Technology, China (2011B050400011). BZG also acknowledges the support from the grant established by the State Key Laboratory of Precision Measuring Technology and Instruments (Tianjin University). ZM acknowledges his Siebel Institute Postdoctoral Fellowship (41523-31595-44-OYZHMA-IQKEH).

References

1. Ruiz SA, Chen CS. Emergence of patterned stem cell differentiation within multicellular structures. Stem Cells. 2008; 26:2921–2927. [PubMed: 18703661]
2. Rowlands AS, George PA, Cooper-White JJ. Directing osteogenic and myogenic differentiation of MSCs: interplay of stiffness and adhesive ligand presentation. Am J Physiol Cell Physiol. 2008; 295:C1037–C1044. [PubMed: 18753317]
3. Kilian KA, Bugarija B, Lahn BT, Mrksich M. Geometric cues for directing the differentiation of mesenchymal stem cells. Proc Natl Acad Sci USA. 2010; 107:4872–4877. [PubMed: 20194780]
4. Sung JH, Shuler ML. Microtechnology for mimicking *in vivo* tissue environment. Ann Biomed Eng. 2012; 40:1289–1300. [PubMed: 22215276]
5. Park JY, Takayama S, Lee SH. Regulating microenvironmental stimuli for stem cells and cancer cells using microsystems. Integr Biol. 2010; 2:229–240.
6. Scanlon MJ, Ohtsu K, Timmermans MC, Schnable PS. Laser microdissection-mediated isolation and *in vitro* transcriptional amplification of plant RNA. Curr Protoc Mol Biol. 2009 Chapter 25: Unit 25A 3.
7. Li Y, Thompson H, Hemphill C, Hong F, Forrester J, et al. An improved one-tube RT-PCR protocol for analyzing single-cell gene expression in individual mammalian cells. Anal Bioanal Chem. 2010; 397:1853–1859. [PubMed: 20490471]
8. Di Carlo D, Wu LY, Lee LP. Dynamic single cell culture array. Lab Chip. 2006; 6:1445–1449. [PubMed: 17066168]
9. Sussman MA, Murry CE. Bones of contention: marrow-derived cells in myocardial regeneration. J Mol Cell Cardiol. 2008; 44:950–953. [PubMed: 18440020]
10. Laflamme MA, Zbinden S, Epstein SE, Murry CE. Cell-based therapy for myocardial ischemia and infarction: pathophysiological mechanisms. Annu Rev Pathol. 2007; 2:307–339. [PubMed: 18039102]
11. Pittenger MF, Martin BJ. Mesenchymal stem cells and their potential as cardiac therapeutics. Circ Res. 2004; 95:9–20. [PubMed: 15242981]
12. Pijnappels DA, Schalij MJ, Ramkisoensing AA, van Tuyn J, de Vries AA, et al. Forced alignment of mesenchymal stem cells undergoing cardiomyogenic differentiation affects functional integration with cardiomyocyte cultures. Circ Res. 2008; 103:167–176. [PubMed: 18556577]
13. Klinger R, Bursac N. Cardiac cell therapy *in vitro*: reproducible assays for comparing the efficacy of different donor cells. IEEE Eng Med Biol Mag. 2008; 27:72–80. [PubMed: 18270054]
14. Pedrotty DM, Klinger RY, Badie N, Hinds S, Kardashian A, et al. Structural coupling of cardiomyocytes and noncardiomyocytes: quantitative comparisons using a novel micropatterned cell pair assay. Am J Physiol Heart Circ Physiol. 2008; 295:H390– H400. [PubMed: 18502901]
15. Pirlo RK, Ma Z, Sweeney A, Liu H, Yun JX, et al. Laser-guided cell micropatterning system. Rev Sci Instrum. 2011; 82:013708. [PubMed: 21280838]
16. Geisse NA, Sheehy SP, Parker KK. Control of myocyte remodeling *in vitro* with engineered substrates. In Vitro Cell Dev Biol Anim. 2009; 45:343–350. [PubMed: 19252956]
17. Ma Z, Pirlo RK, Wan Q, Yun JX, Yuan X, et al. Laser-guidance-based cell deposition microscope for heterotypic single-cell micropatterning. Biofabrication. 2011; 3:034107. [PubMed: 21725149]
18. Ashkin A. Forces of a single-beam gradient laser trap on a dielectric sphere in the ray optics regime. Methods Cell Biol. 1998; 55:1–27. [PubMed: 9352508]
19. Ren KF, Grehan G, Gouesbet G. Prediction of reverse radiation pressure by generalized Lorenz–Mie theory. Appl Opt. 1996; 35:2702–2710. [PubMed: 21085418]

NIH-PA Author Manuscript

NIH-PA Author Manuscript

NIH-PA Author Manuscript

20. Nahmias YK, Gao BZ, Odde DJ. Dimensionless parameters for the design of optical traps and laser guidance systems. Appl Opt. 2004; 43:3999–4006. [PubMed: 15285089]

21. Ma Z, Liu Q, Liu H, Yang H, Yun JX, et al. Laser-patterned stem-cell bridges in a cardiac muscle model for on-chip electrical conductivity analyses. Lab Chip. 2012; 12:566–573. [PubMed: 22170399]

22. Nahmias Y, Odde DJ. Analysis of radiation forces in laser trapping and laser-guided direct writing applications. IEEE J Quantum Electron. 2002; 38:131–141.

23. de Boer TP, van Veen TA, Jonsson MK, Kok BG, Metz CH, et al. Human cardiomyocyte progenitor cell-derived cardiomyocytes display a maturated electrical phenotype. J Mol Cell Cardiol. 2010; 48:254–260. [PubMed: 19460390]

NIH-PA Author Manuscript
NIH-PA Author Manuscript
NIH-PA Author Manuscript

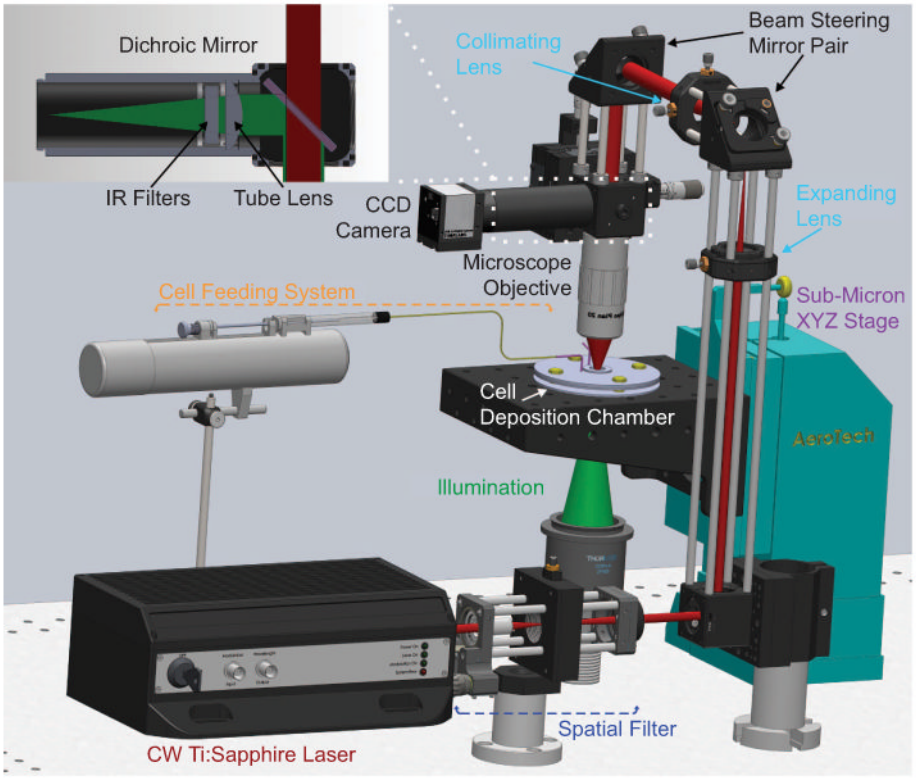

Figure 1.
The laser-guided cell micropatterning system. The inserted plot shows the light path inside the dichroic cube. Red indicates the laser beam used for cell micropatterning, and green indicates the illumination light.

NIH-PA Author Manuscript
NIH-PA Author Manuscript
NIH-PA Author Manuscript

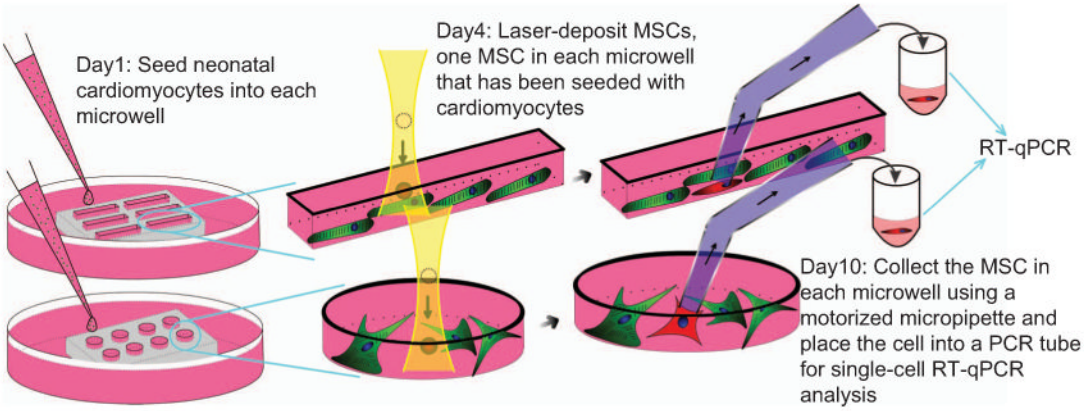

Figure 2.

A schematic of the experimental procedures: rat neonatal cardiomyocytes are seeded into microwells microfabricated on PDMS-based biochips, which are placed inside 35-mm cell culture dishes with one chip per dish. The Rectangular (200 μm long and 25 μm wide) and circular (80 μm in diameter) microwells are designed for constructing aligned and random coculture models, respectively. A single rat mesenchymal stem cell is then deposited into each microwell at the space surrounded by the neonatal cardiomyocytes. Finally, immunostaining, single-cell PCR and patch clamp assays are performed on the biochips. MSC, mesenchymal stem cell; PCR, polymerase chain reaction; PDMS, polydimethylsiloxane.

NIH-PA Author Manuscript

NIH-PA Author Manuscript

NIH-PA Author Manuscript

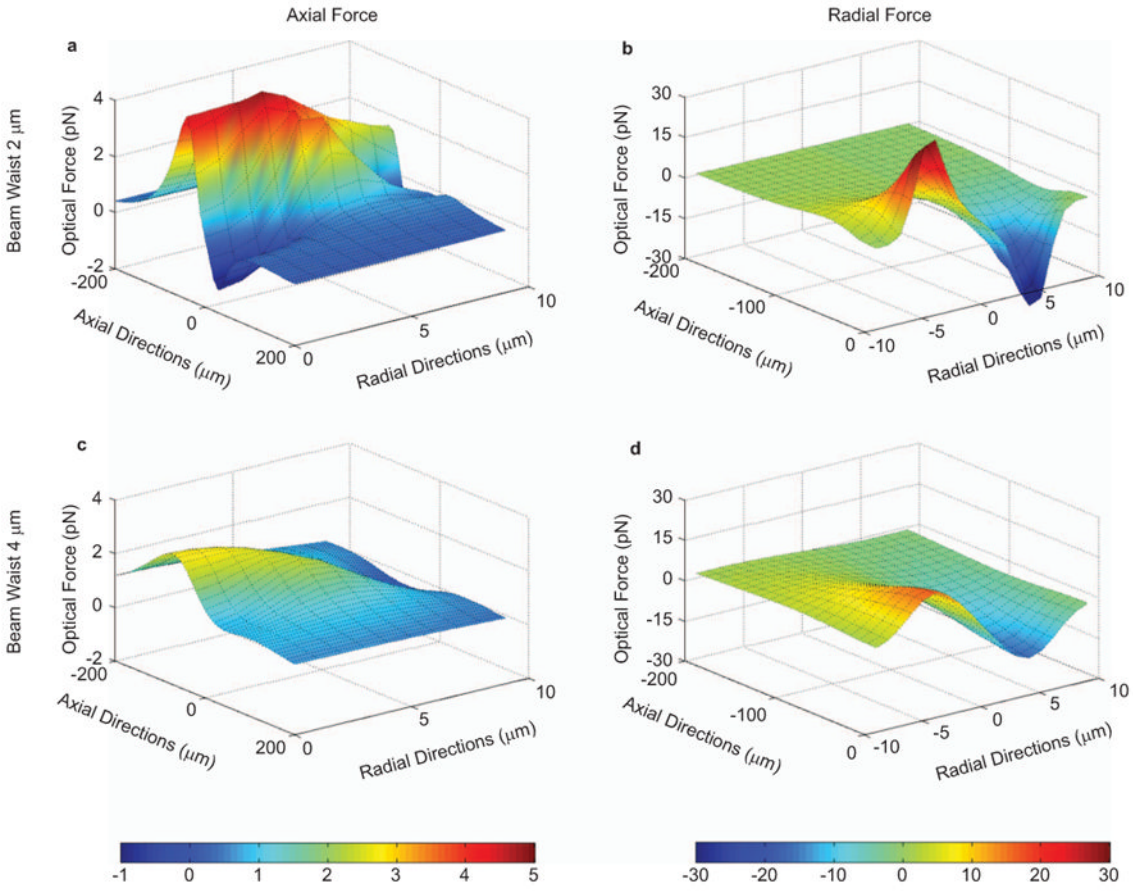

Figure 3.

The optical force distribution was theoretically calculated along the axial and radial directions with different beam waists. (**a**) The axial force distribution with a beam waist of 2 μm; (**b**) the radial force distribution with a beam waist of 2 μm; (**c**) the axial force distribution with a beam waist of 4 μm; (**d**) the radial force distribution with a beam waist of 4 μm.

NIH-PA Author Manuscript

NIH-PA Author Manuscript

NIH-PA Author Manuscript

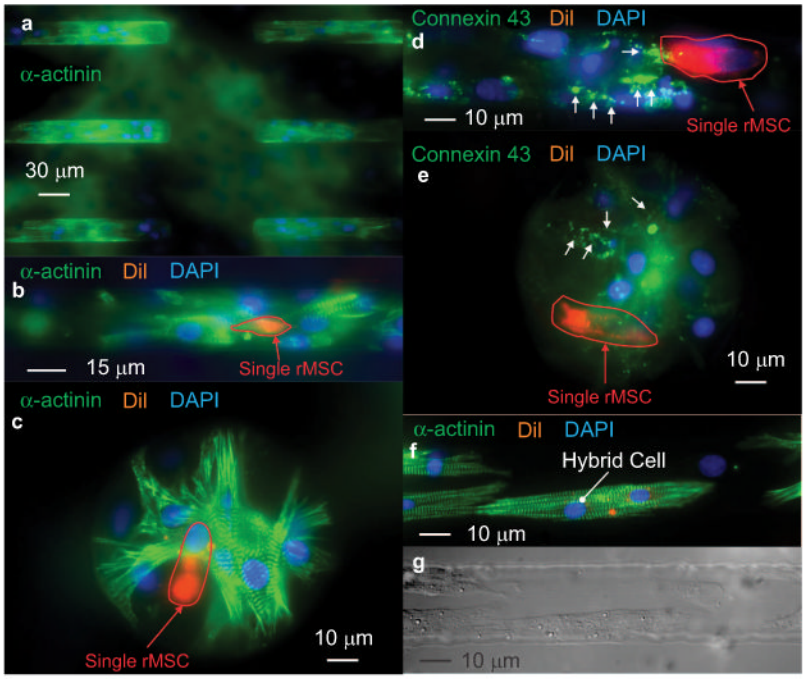

Figure 4.

Confocal images of the immunostained cells inthe microwells. (**a**) A portion of a biochip developed as an aligned coculture model; (**b**) an rMSC aligned with its surrounding cardiomyocytes inside a rectangular microwell; (**c**) a randomly spread rMSC inside a circular microwell; (**d**) an *in vivo*-like Cx 43 distribution between the rMSC and the surrounding cardiomyocytes; (**e**) an irregularly distributed Cx 43 expression; (**f**) cell fusion revealed by hybrid DiI-labeling, featuring the double nuclei and sarcomeric structures; (**g**) the corresponding phase-contrast image of the fused cell. The red circles represent the rMSC cell boundary traced from the corresponding phase images simultaneously obtained from the same confocal microscope. The white arrows point to Cx 43. rMSC, rat bone marrow mesenchymal stem cell.

NIH-PA Author Manuscript

NIH-PA Author Manuscript

NIH-PA Author Manuscript

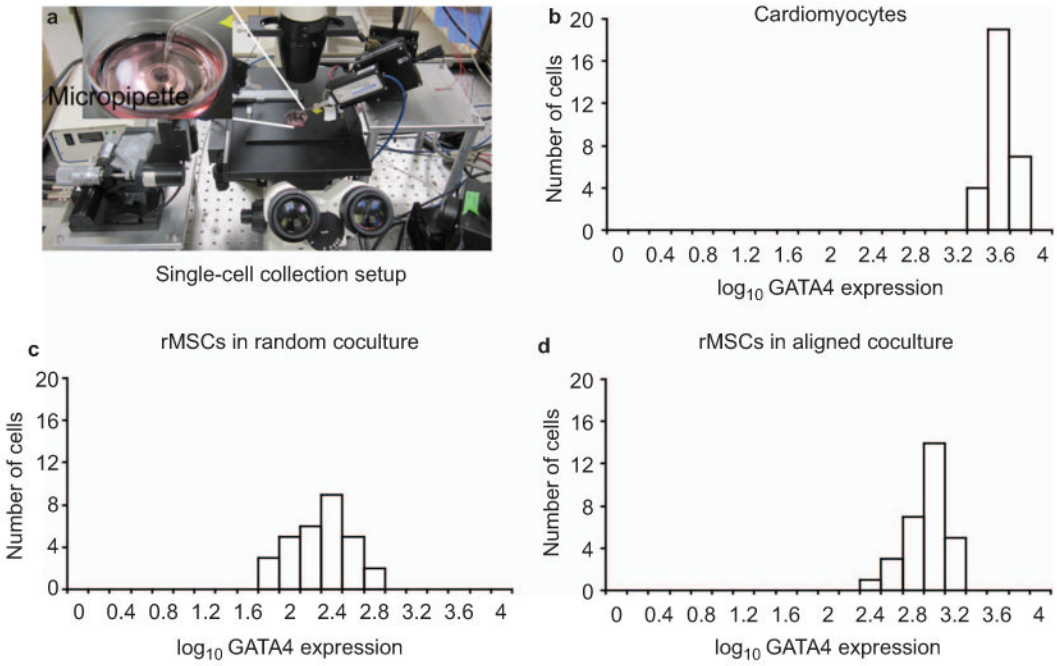

Figure 5.
The single-cell RT-qPCR analysis of GATA4 expression. (**a**) The system for single-cell PCR extraction. The GATA4 gene expression distribution was plotted in logarithmic scale for (**b**) cocultured cardiomyocytes, (**c**) rMSCs in a non-aligned coculture and (d) rMSCs in an aligned coculture. PCR, polymerase chain reaction; rMSC, rat bone marrow mesenchymal stem cell.

NIH-PA Author Manuscript
NIH-PA Author Manuscript
NIH-PA Author Manuscript

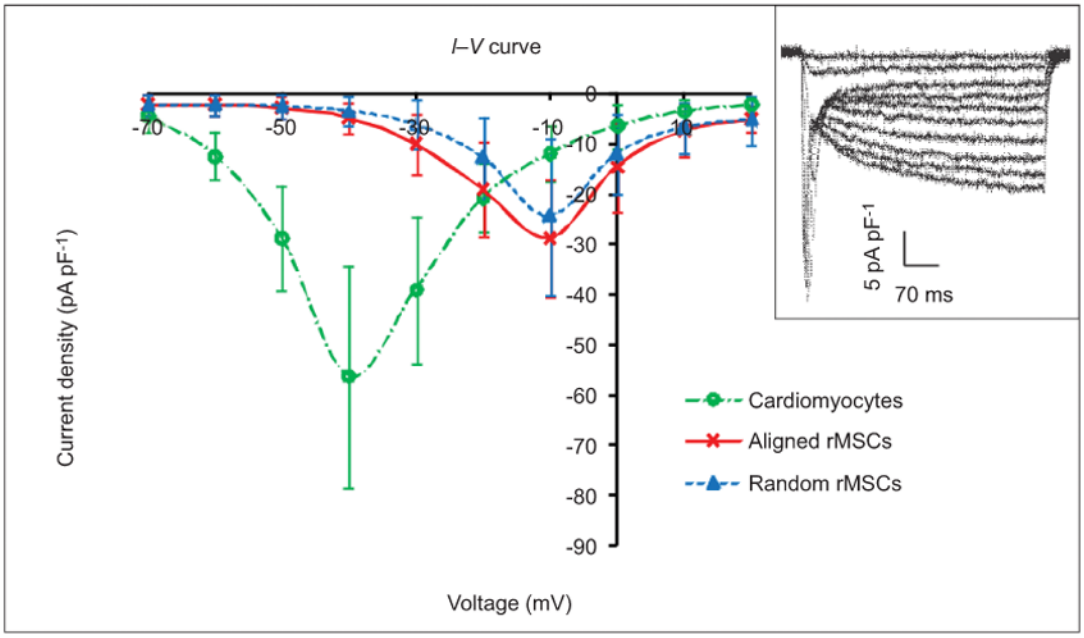

Figure 6.
Current–voltage (*I–V*) curves of the rMSCs and cocultured cardiomyocytes. The *I–V* curves demonstrate the difference between the aligned and random coculture models in inward current density at the different cell membrane potentials of the rMSCs. The inserted plot shows a typical patch-clamp recording obtained with a voltage-step protocol. rMSC, rat bone marrow mesenchymal stem cell.